ACS APPLIED MATERIALS & INTERFACES

Research Article

www.acsami.org

Hollow Structured Silicon Anodes with Stabilized Solid Electrolyte Interphase Film for Lithium-Ion Batteries

Qiuliang Lv, Yuan Liu, Tianyi Ma, Wentao Zhu, and Xinping Qiu*

Key Laboratory of Organic Optoelectronics and Molecular Engineering, Department of Chemistry, Tsinghua University, Beijing 100084, China

Supporting Information

ABSTRACT: Silicon has been considered as a promising anode material for the next generation of lithium-ion batteries due to its high specific capacity. Its huge volume expansion during the alloying reaction with lithium spoils the stability of the interface between electrode and electrolyte, resulting in capacity degradation. Herein, we synthesized a novel hollow structured silicon material with interior space for accumulating the volume change during the lithiation. The as-prepared material shows excellent cycling stability, with a reversible capacity of ~1650 m Ah g^{-1} after 100 cycles, corresponding to 92% retention. The electrochemical impedance spectroscopy and differential scanning calorimetry were carried out to monitor the growth of SEI film, and the results confirm the stable solid electrolyte interphase film on the surface of hollow structured silicon.

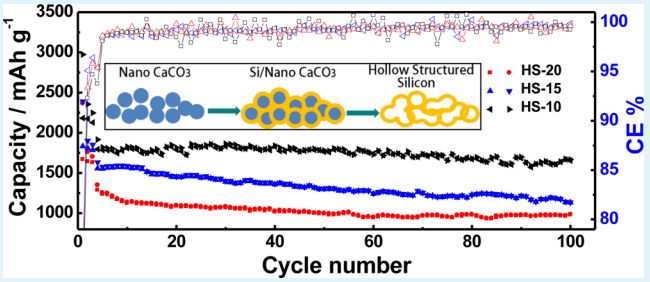

KEYWORDS: *anode, silicon, Coulombic efficiency, interface stability, lithium-ion battery*

INTRODUCTION

Silicon has been regarded as a promising anode material for the next generation of lithium-ion batteries (LIBs)[1−4] due to its low discharge potential and high specific capacity. However, huge volume expansion during the alloying reaction with lithium causes the pulverization of particles, disintegration of electrodes,[5−7] and rupture of the existing interface layer, which promotes the continual formation of SEI film. Excessive growth of SEI film, observed in previous work,[8,9] results from the increase of impedance, irreversible capacity loss, and low Coulombic efficiency during cycle.[10−12] The anode with low Coulombic efficiency continuously consumes lithium ions from the cathode and causes rapid capacity degradation of the balanced full battery.

Nanostructured silicon materials, such as hollow nanospheres,[13−15] silicon core and hollow carbon shell nanocomposites,[16−19] and 1D hollow silicon nanotubes,[20−23] with void inside have been reported to have improved cycle performance. Voids in the materials can efficiently accommodate the large strain from the lithiation and dethiathtion reaction. The nanostructure can also absorb the electrolyte and shorten the diffusion paths of lithium ions, which are beneficial for rate capability. In spite of the enhanced electrochemical performance, the direct and effective characterization of SEI film stability is still absent of evidence; in addition, the vital process of engineering the voids in these materials is not very efficient. In this work, we report a facile approach to preparing hollow structured silicon material through a chemical vapor deposition (CVD) method with calcium carbonate ($CaCO_3$) as the template. With the built-in space, this product presents a remarkable capacity retention and fairly high Coulombic efficiency. The stablity of SEI film is demonstrated as well.

EXPERIMENTAL SECTION

Preparation of Hollow Structured Silicon Material. Commercial nanostructured $CaCO_3$ (ShanXi NanoMaterials Technology Co., Ltd.) was directly used as the template in CVD process. Silicon deposition was conducted in a horizontal tube furnace at 480 °C with mixed gas of 5 wt % SiH_4 and Ar as silicon source. The wall thickness of the silicon form was controlled by the time of deposition and the samples denoted as HS-10, HS-15, and HS-20 corresponding to the deposition time of 1, 1.5, and 2 h, respectively. The $CaCO_3$ template was removed with hydrochloric acid (5 wt %). SiO_x on the surface of hollow structured silicon was removed in hydrofluoric acid (10 wt %) solution.

Structural Characterization. Morphologies of samples were observed on a transmission electron microscopy (TEM, JEOL model JEM-2011) operating at 80 keV and a scanning electron microscopy (SEM, HITACHI S-5500) operating at 5 keV. X-ray diffraction (XRD) spectra were collected using an X-ray diffractometer (Bruker D8 Advance) with a Cu Kα radiation source, and values of 2θ were scanned in the range of 10° to 90° at a rate of 8° min^{-1} with a step of 0.02°. X-ray photoelectron spectroscopy (XPS) measurements were conducted with a PHI Quantera SXM spectrometer using a focused and monochromatized Al Kα radiation, and the binding energy scale was calibrated using the C 1s peak at 284.8 eV. N_2 sorption measurements were carried out on a Quantachrome NOVA 1000e at 77.3 K. Specific surface area and pore-size distribution were

Received: July 3, 2015
Accepted: September 24, 2015
Published: September 24, 2015

DOI: 10.1021/acsami.5b05970
ACS Appl. Mater. Interfaces 2015, 7, 23501−23506

calculated using the Brunauer–Emmett–Teller (BET) and Barrett–Joyner–Halenda (BJH) methods, respectively. The differential scanning calorimetry (DSC) was performed on a Mettler-Toleda 821 calorimeter. The Li_xSi material was scratched from the electrode in the argon glovebox and sealed in a hermetic high-pressure stainless steel gold-plated crucible (Mettler Toledo). DSC measurements were performed from 30 to 300 °C at a temperature ramp of 2 °C min^{-1}.

Electrochemical Measurements. The electrodes for electrochemical tests were prepared by coating slurries (containing 80 wt % active material, 10 wt % carbon black (Super P Li, TIMCAL), and 10 wt % poly(acrylic acid) (PAA)) onto copper foil. The loading of active materials in the electrode is 0.4–0.6 mg cm^{-2}. 2025 coin cells were assembled with lithium foil as the counter electrode. The electrolyte solution was composed of 1 M $LiPF_6$ dissolved in a nonaqueous mixture of ethylene carbonate/dimethyl carbonate/ethylmethyl carbonate (EC/DMC/EMC, 1:1:1 volume ratio) with 2.5 wt % vinylene carbonate (VC) as an additive (Zhangjiagang Guotai-Huarong New Chemical Materials Co., Ltd.). Galvanostatic tests were performed between 0.05 and 1.5 V versus Li/Li^+ with a relaxation period of 1 min at the end of each charge and discharge process. A total of three electrode cells (ECC-REF model, EL-CELL) were assembled for electrochemical impedance spectra (EIS) tests using Li foil as the reference and counter electrodes. EIS measurements were conducted on a PARSTAT2273 electrochemical workstation (AMETEK). The AC potential was controlled with an amplitude of 5.0 mV in the frequency range of 10^5–0.02 Hz. Before the tests, a constant current density of 100 mA g^{-1} was applied in the discharge process until the voltage reached 1 mV versus Li/Li^+, and then the cells remained at an open-circuit state for 2 h to stabilize their potential. All cells were assembled in an Ar-filled glovebox with moisture and oxygen contents below 1 ppm.

RESULTS AND DISCUSSION

We fabricated hollow structured silicon with a simple template method, as illustrated in Figure 1. The silicon was deposited

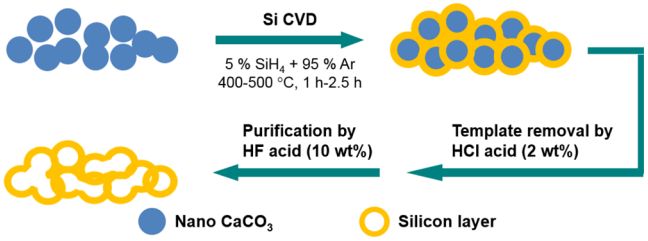

Figure 1. Schematic diagram of the fabrication process of porous silicon.

onto a nanosized $CaCO_3$ template by a CVD process. The $CaCO_3$ template was washed away in hydrochloric acid solution. The resulting silicon was then treated in hydrofluoric acid to remove the SiO_x. The morphology of nanosized $CaCO_3$ particles is nearly spherical in shape, as shown in panels a and b of Figure 2, with a narrowly distributed particle size of 50 nm. After deposition, a layer of silicon can be observed on the surface of nanosized $CaCO_3$ (Figure 2c,d). An interconnected hollow structured silicon material was left after the removal of the template in hydrochloric acid (Figure 2e,f).

The wall thickness of porous silicon can be tailored by the control of time of CVD in a fixed flow rate of the precursor gas. TEM images in Figure 3 show that the wall thickness in the hollow structured silicon increases with the deposition time. Broad diffuse rings in the selected-area electron diffraction (SAED) pattern of the HS-10 sample (inset of Figure 3a) reveal that silicon is amorphous. In the XRD patterns of all samples, as shown in Figure 3d, characteristic peaks of crystalline silicon

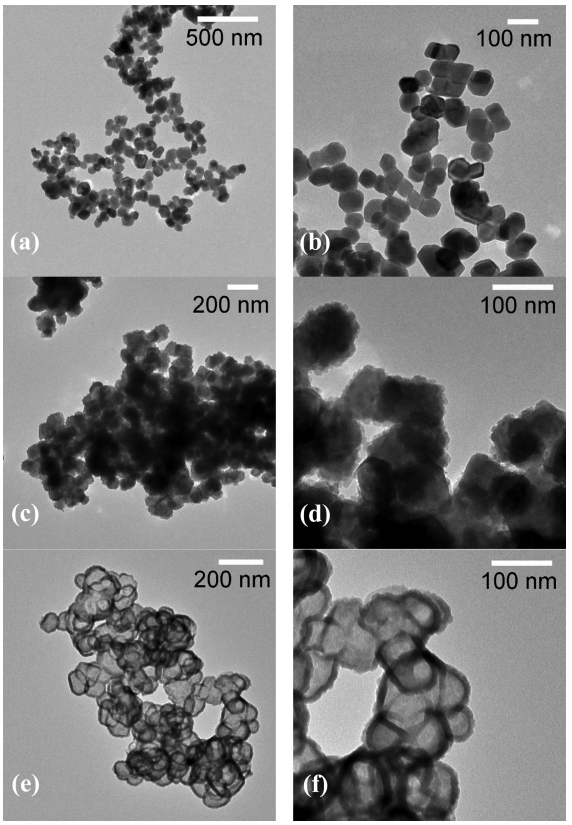

Figure 2. Transmission electron microscopy images of (a,b) nano $CaCO_3$, (c,d) $CaCO_3$ deposited with silicon layer, and (e,f) hollow structured silicon.

(PDF#65-1060) around 28°, 47°, and 56° are absent, indicating the amorphous structure of silicon, in agreement with the results of SAED. The XPS spectra of Si 2p in Figure 3e are fitted well using a nonlinear Shirley-type background[24] and a combination of 80% Gaussian and 20% Lorentzian line shapes. The first main 3/2–1/2 doublet (the spin–orbit splitting is 0.6 eV and the intensity ratio is 3:1), located at 99.1–99.7 eV, corresponds to Si^0 (75% content). The component located at a higher binding energy (100.0 eV) is associated with SiO_x formed on the surface, with a proportion of 25%.[25] The nitrogen adsorption and desorption isotherms inFigure S1a show a sharp capillary condensation step at high relative pressures (P/P_0 = 0.85–0.99), indicating the existence of large pores. Corresponding pore size distributes mainly in the range of 20 to 100 nm (Figure S1b), which is attributed to the removal of the site-occupying $CaCO_3$ template. With the increase of silicon wall thickness, the specific surface area and pore volume decrease obviously (Table S1) owing to the integrated silicon layer and increased density of material.

Galvanostatic tests were performed at a constant current densities of 100 mA g^{-1} for the first three cycles and 500 mA g^{-1} for later cycles. The specific capacity was calculated based on the mass of silicon. Figure 4a shows the first and second charge and discharge profiles of HS-10 at a rate of 100 mA/g. A long platform is observed in the first discharge process and disappeared in subsequent cycles, corresponding to the SEI film formation.[26] The sloping voltage profile suggests a typical lithiation reaction of amorphous silicon.[6,27] For the first discharge-and-charge cycle, the capacities reach 2973 and 2367 mAh g^{-1}, respectively, corresponding to the Coulombic

DOI: 10.1021/acsami.5b05970
ACS Appl. Mater. Interfaces 2015, 7, 23501–23506

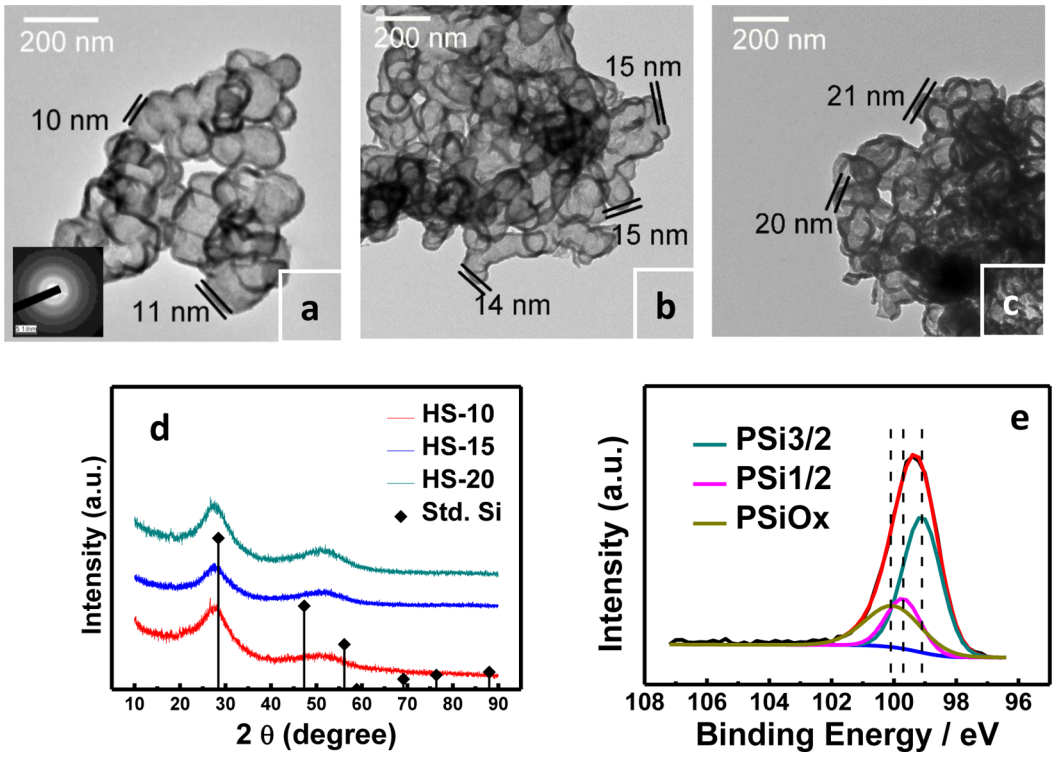

Figure 3. TEM images of hollow structured silicon with different thicknesses: (a) HS-10 (inset is the corresponding selected-area electron diffraction pattern), (b) HS-15, (c) HS-20, (d) X-ray power diffraction patterns of HS samples, and (e) X-ray photoelectron spectroscopy analysis of Si 2p of HS-10.

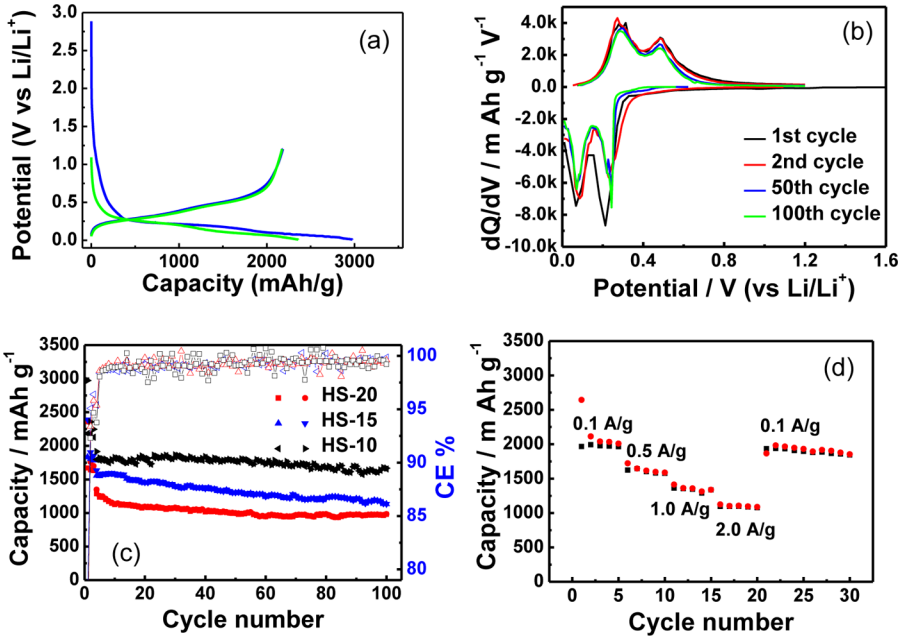

Figure 4. Electrochemical performance of hollow structured silicon samples. (a) Charge and discharge voltage profiles of HS-10 at a 0.1A/g rate in the first two cycles. (b) Differential capacity of HS-10 in different cycles. (c) Capacity retention during 100 cycles for HS-10, HS-15, and HS-20. (d) Capacity of HS-10 at various charge and discharge rates.

efficiency of 73.4%. Plots of the differential capacity of HS-10 in different cycles are presented in Figure 3b. The peak at 0.2 V in the first discharge suggests the lithiation process in amorphous silicon. During the first charge, two peaks at 0.32 and 0.48 V indicate the formation of amorphous silicon during the dealloying reaction, this being consistent with the previous report in the literature for amorphous silicon electrodes.[14,28−30] Peak values from 50 to 100 cycles are almost unchanged, indicating little capacity losses during cycling.[15]

Figure 4c illustrates the cycle performance and Coulombic efficiency. Among these samples, HS-10 shows the highest capacity retention (92%) after 100 cycles, corresponding to the reversible capacity of 1654 mAh g^{-1}. The benefit from the short lithium-ion diffusion distance in this nanostructure, excellent

DOI: 10.1021/acsami.5b05970
ACS Appl. Mater. Interfaces 2015, 7, 23501−23506

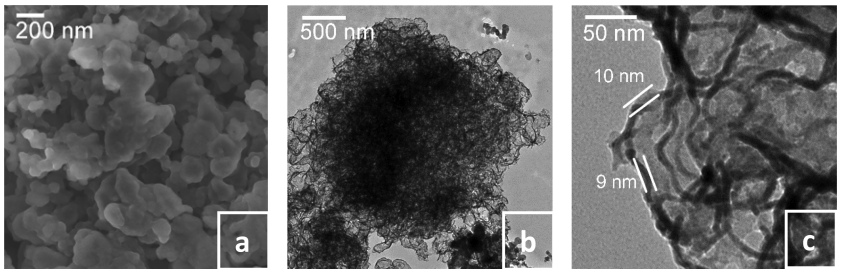

Figure 5. (a) SEM image of HS-10 electrode after 100 cycles and (b,c) TEM images of HS-10 after 100 cycles, where SEI film was washed away.

rate capability, is also demonstrated (Figure 4d). After an increase in the current density from 0.1 to 2 A g^{-1}, the specific capacity of HS-10 becomes more than 1000 m Ah g^{-1}; when the current density changes back to 0.1 A g^{-1}, 98.5% of the capacity of the first cycle is recoverable. The increase of the wall thickness of hollowed silicon decreases the capacity retention obviously (76% for HF-15 and 73% for HS-20 after 100 cycles); this is possible due to the limited interior space for volume change.

To investigate the evolution process of SEI during cycles, we took the HS-10 electrode out of the coin cell after 100 cycles and washed off the electrolyte residue in dimethyl carbonate. Primary hollow structured silicon covered with SEI film can be observed in Figure 5a, and the surface of the hollow structured silicon and the carbon black additives can be clearly distinguished, demonstrating no excessive growth of SEI film. We used 1 mM acetic acid solution to remove the SEI film.[31] The shape (Figure 5b) and the wall (Figure 5c) were maintained without fractures and cracks. This indicates that hollow structured silicon can withstand the volume change.

Electrochemical impedance spectroscopy (EIS) measurements were further conducted. Typical Nyquist plots of hollow structured silicon electrode are illustrated in Figure 6a. The semicircle in the midfrequency regime is generally associated with interfacial phenomena, either the charge transfer or the occurrence of SEI film between the active particles and the liquid electrolyte;[11] the impedance tail in the low-frequency region can be attributed to the bulk diffusional effects. R_{Sur} here is used to evaluate the whole surface resistance (the equivalent circuit is shown in the inset of Figure 6a). In Figure 6a and 6b, R_{Sur} maintains around 20 Ohm for HS-10, which indicates the stable SEI during cycling. After five cycles, the constancy of the characteristic frequency (2.63 kHz) suggests that the kinetics of the charge-transfer reaction and the SEI film conductivity do not change. By contrast, the continuous increase of R_{Sur} is observed for the electrode with Si nanoparticles in our previous research,[32] indicating excessive SEI growth.

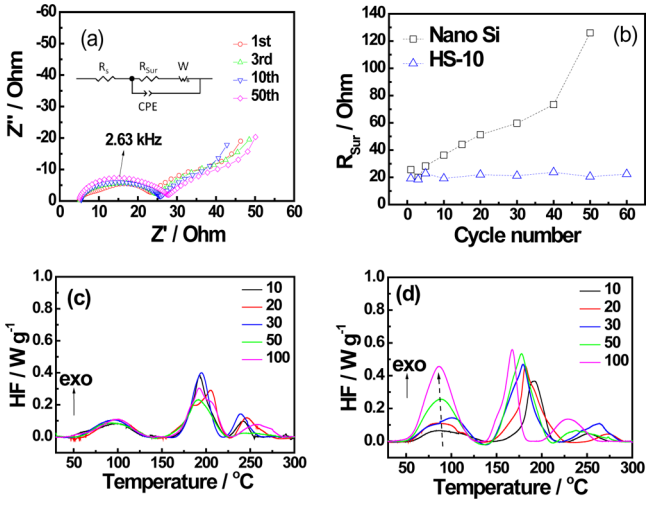

Figure 6. (a) Nyquist plot of HS-10 at the end of discharge after different cycles (inset is the equivalent circuit). (b) The evolution of the resistance of the semicircle. (c,d) DSC curves for HS-10 and nanosized Si after different cycles.

To evaluate the amount of SEI film directly, we developed a method based on differential scanning calorimetry (DSC). In detail, the cells were discharged at a constant current density of 100 mA g^{-1} to the voltage of 1 mV and remained at an open-circuit state for 2 h to stabilize their potential. They were then carefully opened in the glovebox, and the retrieved electrodes were rinsed in dimethyl carbonate solvent to remove the electrolyte and then dried in a vacuum overnight. Li_xSi material was scratched from the electrode and was sealed into a hermetic high-pressure stainless-steel crucible for DSC tests. Figure 6c,d present the DSC curves for lithiated silicon after different cycles. An exothermic signal at 86−100 °C is visible for all the curves of HS-10 and nano Si material. By analogy with the lithiated graphite and nanosized silicon electrode,[33−36] it can be reasonably suggested that these exothermic peaks are attributed to the transformation of metastable SEI layer components. At elevated temperatures, the metastable components in SEI film ($ROCO_2Li$ compounds, ROLi, polycarbonate species, and lithium oxalate)[33,34] decompose and react with lithium in Li_xSi.

For nanosized Si, much larger exothermic heat at 86−100 °C is observed, indicating that the amount of SEI film increases continuously. Meanwhile, there is no obvious change of the exothermic peak for HS-10, which suggests that SEI formation in hollow structured silicon is confined and that the interface layer between electrode and electrolyte is more stable. Another remarkable phenomenon is that the peak position at higher temperatures (167−190 °C) shows a shift to low temperatures for nanosized Si material. According to previous literature,[36−38] this peak can be associated with the conversion of metastable α-Li_xSi phases to thermodynamically stable ones, where lithium content (x value) is account for the shape and position of the peak. The continuous formation of SEI film on nanosized Si consumes more lithium in the reaction, resulting in a decreased x value in α-Li_xSi and a further shift of the peak position.[37,38] In HS-10, exothermic peaks of α-Li_xSi conversion maintain a similar shape and position, which confirm that the interface stability in hollow structured silicon material is much better.

In summary, hollow structured silicon material is synthesized using a facile chemical-vapor deposition method in combination with nanosized calcium carbonate as a template. The influence of silicon shell thickness on electrochemical perform-

DOI: 10.1021/acsami.5b05970
ACS Appl. Mater. Interfaces 2015, 7, 23501−23506

ance have been discussed. This material exhibits excellent cycling stability and rate performance without crushing the hollow structure. The Coulombic efficiency during cycling is maintained at nearly 100%, which is beneficial for a long cycle life. Furthermore, EIS and DSC observations on the SEI film transformation lead us to a deeper understanding of the interface stability. Considering the fact that nanosized calcium carbonate is commercially available,[39] this hollow structured silicon material is a promising anode candidate for the next generation of lithium-ion batteries.

■ ASSOCIATED CONTENT

Supporting Information

The Supporting Information is available free of charge on the ACS Publications website at DOI: 10.1021/acsami.5b05970.

Image showing the nitrogen sorption isotherms of silicon foam samples and corresponding pore-size distributions and a table showing the specific surface area and pore volume of HS samples. (PDF)

■ AUTHOR INFORMATION

Corresponding Author

*E-mail: qiuxp@mail.tsinghua.edu.cn; tel: +86-10-62794234; fax: +86-10-62794234.

Notes

The authors declare no competing financial interest.

■ ACKNOWLEDGMENTS

The authors appreciate the support from the National Key Project on Basic Research (2013CB934000 and 2015CB251104), the National International Science and Technology Cooperation Project (2012DFG61480), the China−Germany Electric Vehicle Project (2011AA11A290), the China−US Electric Vehicle Project (2010DFA72760) ,the Beijing Natural Science Foundation (2120001), and the Tsinghua University independent research program (20111081039).

■ REFERENCES

(1) Huggins, R. A. Lithium alloy negative electrodes. *J. Power Sources* **1999**, *81*, 13−19.
(2) Park, C.-M.; Kim, J.-H.; Kim, H.; Sohn, H.-J. Li-alloy based anode materials for Li secondary batteries. *Chem. Soc. Rev.* **2010**, *39*, 3115−3141.
(3) McDowell, M. T.; Lee, S. W.; Nix, W. D.; Cui, Y. 25th Anniversary Article: Understanding the Lithiation of Silicon and Other Alloying Anodes for Lithium-Ion Batteries. *Adv. Mater.* **2013**, *25*, 4966−4984.
(4) Su, X.; Wu, Q.; Li, J.; Xiao, X.; Lott, A.; Lu, W.; Sheldon, B. W.; Wu, J. Silicon-Based Nanomaterials for Lithium-Ion Batteries: A Review, Adv. *Energy Mater.* **2014**, *4*, 882.
(5) Beaulieu, L. Y.; Eberman, K. W.; Turner, R. L.; Krause, L. J.; Dahn, J. R. Colossal reversible volume changes in lithium alloys, Electrochem. *Electrochem. Solid-State Lett.* **2001**, *4*, A137−A140.
(6) Beaulieu, L. Y.; Hatchard, T. D.; Bonakdarpour, A.; Fleischauer, M. D.; Dahn, J. R. Reaction of Li with alloy thin films studied by in situ AFM. *J. Electrochem. Soc.* **2003**, *150*, A1457−A1464.
(7) Jerliu, B.; Hüger, E.; Dörrer, L.; Seidlhofer, B. K.; Steitz, R.; Oberst, V.; Geckle, U.; Bruns, M.; Schmidt, H. Volume Expansion during Lithiation of Amorphous Silicon Thin Film Electrodes Studied by In-Operando Neutron Reflectometry. *J. Phys. Chem. C* **2014**, *118*, 9395−9399.
(8) Nie, M.; Abraham, D. P.; Chen, Y.; Bose, A.; Lucht, B. L. Silicon Solid Electrolyte Interphase (SEI) of Lithium Ion Battery Characterized by Microscopy and Spectroscopy. *J. Phys. Chem. C* **2013**, *117*, 13403−13412.
(9) Cho, J.-H.; Picraux, S. T. Silicon Nanowire Degradation and Stabilization during Lithium Cycling by SEI Layer Formation. *Nano Lett.* **2014**, *14*, 3088−3095.
(10) Mazouzi, D.; Delpuech, N.; Oumellal, Y.; Gauthier, M.; Cerbelaud, M.; Gaubicher, J.; Dupre, N.; Moreau, P.; Guyomard, D.; Roue, L.; Lestriez, B. New insights into the silicon-based electrode's irreversibility along cycle life through simple gravimetric method. *J. Power Sources* **2012**, *220*, 180−184.
(11) Oumellal, Y.; Delpuech, N.; Mazouzi, D.; Dupre, N.; Gaubicher, J.; Moreau, P.; Soudan, P.; Lestriez, B.; Guyomard, D. The failure mechanism of nano-sized Si-based negative electrodes for lithium ion batteries. *J. Mater. Chem.* **2011**, *21*, 6201−6208.
(12) Delpuech, N.; Dupre, N.; Mazouzi, D.; Gaubicher, J.; Moreau, P.; Bridel, J. S.; Guyomard, D.; Lestriez, B. Correlation between irreversible capacity and electrolyte solvents degradation probed by NMR in Si-based negative electrode of Li-ion cell. *Electrochem. Commun.* **2013**, *33*, 72−75.
(13) Esmanski, A.; Ozin, G. A. Silicon Inverse-Opal-Based Macroporous Materials as Negative Electrodes for Lithium Ion Batteries. *Adv. Funct. Mater.* **2009**, *19*, 1999−2010.
(14) Yao, Y.; McDowell, M. T.; Ryu, I.; Wu, H.; Liu, N.; Hu, L.; Nix, W. D.; Cui, Y. Interconnected Silicon Hollow Nanospheres for Lithium-Ion Battery Anodes with Long Cycle Life. *Nano Lett.* **2011**, *11*, 2949−2954.
(15) Chen, D.; Mei, X.; Ji, G.; Lu, M.; Xie, J.; Lu, J.; Lee, J. Y. Reversible Lithium-Ion Storage in Silver-Treated Nanoscale Hollow Porous Silicon Particles, Angew. Chem. *Angew. Chem., Int. Ed.* **2012**, *51*, 2409−2413.
(16) Liu, N.; Wu, H.; McDowell, M. T.; Yao, Y.; Wang, C.; Cui, Y. A Yolk-Shell Design for Stabilized and Scalable Li-Ion Battery Alloy Anodes. *Nano Lett.* **2012**, *12*, 3315−3321.
(17) Li, X.; Meduri, P.; Chen, X.; Qi, W.; Engelhard, M. H.; Xu, W.; Ding, F.; Xiao, J.; Wang, W.; Wang, C.; Zhang, J.-G.; Liu, J. Hollow core-shell structured porous Si-C nanocomposites for Li-ion battery anodes. *J. Mater. Chem.* **2012**, *22*, 11014−11017.
(18) Chen, S.; Gordin, M. L.; Yi, R.; Howlett, G.; Sohn, H.; Wang, D. Silicon core-hollow carbon shell nanocomposites with tunable buffer voids for high capacity anodes of lithium-ion batteries. *Phys. Chem. Chem. Phys.* **2012**, *14*, 12741−12745.
(19) Park, Y.; Choi, N.-S.; Park, S.; Woo, S. H.; Sim, S.; Jang, B. Y.; Oh, S. M.; Park, S.; Cho, J.; Lee, K. T. Si-Encapsulating Hollow Carbon Electrodes via Electroless Etching for Lithium-Ion Batteries, Adv. *Energy Mater.* **2013**, *3*, 206−212.
(20) Hertzberg, B.; Alexeev, A.; Yushin, G. Deformations in Si-Li Anodes Upon Electrochemical Alloying in Nano-Confined Space. *J. Am. Chem. Soc.* **2010**, *132*, 8548−8459.
(21) Yoo, J.-K.; Kim, J.; Jung, Y. S.; Kang, K. Scalable Fabrication of Silicon Nanotubes and their Application to Energy Storage. *Adv. Mater.* **2012**, *24*, 5452−5456.
(22) Wu, H.; Chan, G.; Choi, J. W.; Ryu, I.; Yao, Y.; McDowell, M. T.; Lee, S. W.; Jackson, A.; Yang, Y.; Hu, L.; Cui, Y. Stable cycling of double-walled silicon nanotube battery anodes through solid-electrolyte interphase control, Nat. *Nat. Nanotechnol.* **2012**, *7*, 309−314.
(23) Wang, B.; Li, X.; Zhang, X.; Luo, B.; Zhang, Y.; Zhi, L. Contact-Engineered and Void-Involved Silicon/Carbon Nanohybrids as Lithium-Ion-Battery Anodes. *Adv. Mater.* **2013**, *25*, 3560−3565.
(24) Shirley, D. A. HIGH-RESOLUTION X-RAY PHOTOEMISSION SPECTRUM OF VALENCE BANDS OF GOLD. *Phys. Rev. B* **1972**, *5*, 4709−4714.
(25) Himpsel, F. J.; Mcfeely, F. R.; Talebibrahimi, A.; Yarmoff, J. A.; Hollinger, G. Microscopic Structure Of the Sio2/Si Interface. *Phys. Rev. B: Condens. Matter Mater. Phys.* **1988**, *38*, 6084−6096.
(26) SalverDisma, F.; Lenain, C.; Beaudoin, B.; Aymard, L.; Tarascon, J. M. Unique effect of mechanical milling on the lithium intercalation properties of different carbons. *Solid State Ionics* **1997**, *98*, 145−158.

DOI: 10.1021/acsami.5b05970
ACS Appl. Mater. Interfaces 2015, 7, 23501−23506

(27) Key, B.; Morcrette, M.; Tarascon, J.-M.; Grey, C. P. Pair Distribution Function Analysis and Solid State NMR Studies of Silicon Electrodes for Lithium Ion Batteries: Understanding the (De)lithiation Mechanisms. *J. Am. Chem. Soc.* **2011**, *133*, 503−512.
(28) Hatchard, T. D.; Dahn, J. R. In situ XRD and electrochemical study of the reaction of lithium with amorphous silicon. *J. Electrochem. Soc.* **2004**, *151*, A838−A842.
(29) Datta, M. K.; Kumta, P. N. In situ electrochemical synthesis of lithiated silicon-carbon based composites anode materials for lithium ion batteries. *J. Power Sources* **2009**, *194*, 1043−1052.
(30) Wang, W.; Epur, R.; Kumta, P. N. Vertically aligned silicon/carbon nanotube (VASCNT) arrays: Hierarchical anodes for lithium-ion battery. *Electrochem. Commun.* **2011**, *13*, 429−432.
(31) Choi, J. W.; McDonough, J.; Jeong, S.; Yoo, J. S.; Chan, C. K.; Cui, Y. Stepwise Nanopore Evolution in One-Dimensional Nanostructures. *Nano Lett.* **2010**, *10*, 1409−1413.
(32) Dong, J. P.; Yu, X. Q.; Sun, Y.; Liu, L.; Yang, X. Q.; Huang, X. J. Trip lite LiFeSO4F as cathode material for Li-ion batteries. *J. Power Sources* **2013**, *244*, 716−720.
(33) Haik, O.; Ganin, S.; Gershinsky, G.; Zinigrad, E.; Markovsky, B.; Aurbach, D.; Halalay, I. On the Thermal Behavior of Lithium Intercalated Graphites. *J. Electrochem. Soc.* **2011**, *158*, A913−A923.
(34) Richard, M. N.; Dahn, J. R. Accelerating rate calorimetry study on the thermal stability of lithium intercalated graphite in electrolyte I. Experimental. *J. Electrochem. Soc.* **1999**, *146*, 2068−2077.
(35) Profatilova, I. A.; Stock, C.; Schmitz, A.; Passerini, S.; Winter, M. Enhanced thermal stability of a lithiated nano-silicon electrode by fluoroethylene carbonate and vinylene carbonate. *J. Power Sources* **2013**, *222*, 140−149.
(36) Profatilova, I. A.; Langer, T.; Badillo, J. P.; Schmitz, A.; Orthner, H.; Wiggers, H.; Passerini, S.; Winter, M. Thermally Induced Reactions between Lithiated Nano-Silicon Electrode and Electrolyte for Lithium-Ion Batteries. *J. Electrochem. Soc.* **2012**, *159*, A657−A663.
(37) Wang, Y.; Dahn, J. Phase changes in electrochemically lithiated silicon at elevated temperature. *J. Electrochem. Soc.* **2006**, *153*, A2314−A2318.
(38) Chevrier, V. L.; Dahn, H. M.; Dahn, J. R. Activation Energies of Crystallization Events in Electrochemically Lithiated Silicon. *J. Electrochem. Soc.* **2011**, *158*, A1207−A1213.
(39) Chen, J. F.; Wang, Y. H.; Guo, F.; Wang, X. M.; Zheng, C. Synthesis of nanoparticles with novel technology: High-gravity reactive precipitation. *Ind. Eng. Chem. Res.* **2000**, *39*, 948−954.

DOI: 10.1021/acsami.5b05970
ACS Appl. Mater. Interfaces 2015, 7, 23501−23506